ACS APPLIED MATERIALS & INTERFACES

Research Article

Cite This: ACS Appl. Mater. Interfaces 2018, 10, 6887−6894

www.acsami.org

Highly Sensitive and Quality Self-Testable Electrochemiluminescence Assay of DNA Methyltransferase Activity Using Multifunctional Sandwich-Assembled Carbon Nitride Nanosheets

Shiyu Chen,[†,§] Yanqin Lv,[†,§] Yanfei Shen,[‡] Jingjing Ji,[†] Qing Zhou,[†] Songqin Liu,[†] and Yuanjian Zhang*[,†]

[†]Jiangsu Engineering Laboratory of Smart Carbon-Rich Materials and Device, Jiangsu Province Hi-Tech Key Laboratory for Bio-Medical Research, School of Chemistry and Chemical Engineering, Southeast University, Nanjing 211189, China

[‡]Medical School, Southeast University, Nanjing 210009, China

Supporting Information

ABSTRACT: DNA methylation catalyzed by methylase plays a key role in many biological activities. However, developing a highly sensitive, simple, and reliable way for evaluation of DNA methyltransferase (MTase) activity is still a challenge. Here, we report a sandwich-assembled electrochemiluminescence (ECL) biosensor using multifunctional carbon nitride nanosheets (CNNS) to evaluate the Dam MTase activity. The CNNS could not only be used as an excellent substrate to conjugate a large amount of hairpin probe DNA to improve the sensitivity but also be utilized as an internal reliability checker and an analyte reporter in the bottom and top layers of the biosensor, respectively. Such a unique sandwich configuration of CNNS well coupled the advantages of ECL luminophor that were generally assembled in the bottom or top layer in a conventional manner. As a result, the biosensor exhibited an ultralow detection limit down to 0.043 U/mL and a linear range between 0.05 and 80 U/mL, superior to the MTase activity assay in most previous reports. We highlighted the great potential of emerging CNNS luminophor in developing highly sensitive and smart quality self-testable ECL sensing systems using a sandwiched configuration for early disease diagnosis, treatment, and management.

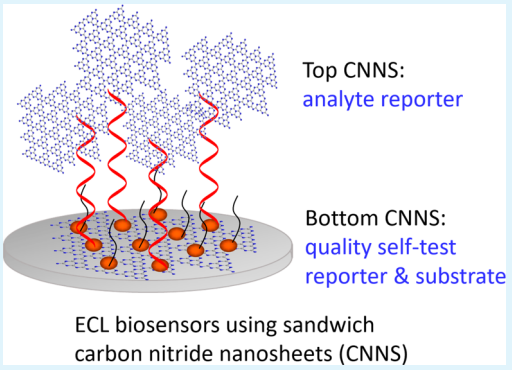

KEYWORDS: *carbon nitride nanosheets, electrochemiluminescence biosensor, DNA methyltransferases, sandwich-assembled structure, quality self-testable*

INTRODUCTION

DNA methylation by methyltransferases (MTase) occurs abundantly in most living organisms and regulates a variety of cellular processes.[1] Recent research reveals that a rapidly growing number of human diseases such as cancers are associated with abnormal DNA methylation.[2,3] Thus, developing a sensitive MTase activity assay is of paramount significance in early disease diagnosis and therapy. Traditional detection methods including high-performance liquid chromatography,[4] gel electrophoresis,[5] and radioactive labeling[6] are golden standards, but they are laborious, time-intensive, and discontinuous and usually require expensive instruments. For this reason, various nanomaterial-derived biosensors using spectroscopic and electrochemical methods are proposed for detecting DNA MTase. For example, spectroscopic methods using the enzyme-responsive DNA−gold nanoparticle (AuNP) assembly[7,8] and electrochemical methods using graphene oxide (GO)/AgNP/luminol composites[9] have been reported to assay the MTase activity, which can partially overcome the above disadvantages but suffer from narrow detection range or low sensitivity. To this end, various polymerase chain reaction (PCR) and isothermal amplification techniques have also been explored;[10−12] nevertheless, the complicated design of DNA sequences and uncertain inhabitation of MTase activity from operating conditions limit their applications. In this regard, developing a highly sensitive, simple, and reliable way for evaluation of DNA MTase activity is still a challenge.

Among those alternatives, electrochemiluminescence (ECL) that is driven by electrochemical generation of excited states, mostly cooperating with coreactants, has drawn numerous attentions for biosensors because of its attractive features such as the absence of photoexcitation background and principally higher signal-to-noise ratio over photoluminescence (PL).[13−19] Of note, as an emerging luminophor for ECL biosensors, semiconducting polymeric carbon nitride (CN), which has been extensively studied for photocatalysis[20,21] and photoelectrochemistry,[22,23] exhibits advantages such as high biocompatibility, controllable band-gap luminescence, and low cost with respect to conventional luminophors such as Ru complex, luminol, and

Received: November 22, 2017
Accepted: January 29, 2018
Published: January 29, 2018

DOI: 10.1021/acsami.7b17813
ACS Appl. Mater. Interfaces 2018, 10, 6887−6894

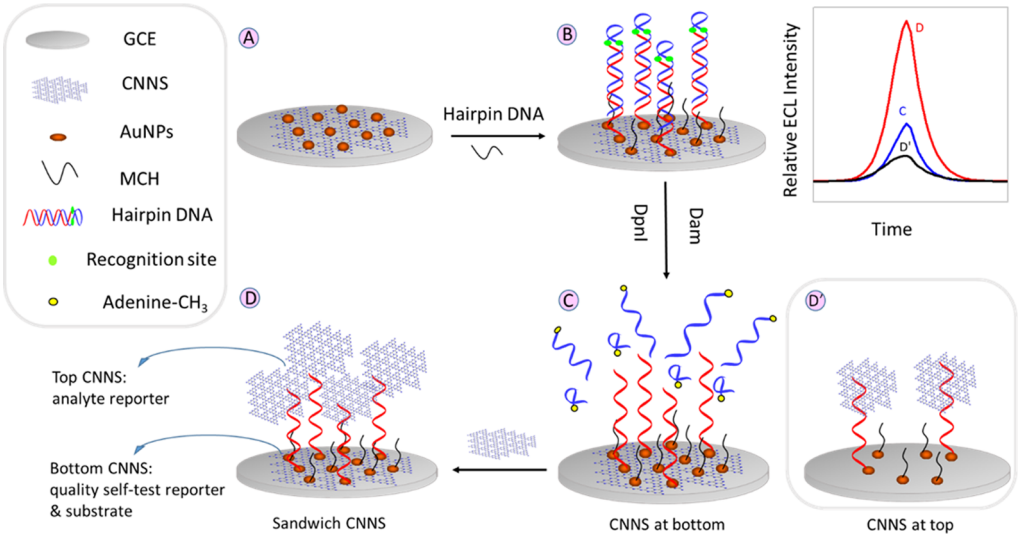

Figure 1. Procedures of assembling the sandwiched CNNS ECL biosensor and the control for evaluating the Dam MTase activity on the glassy carbon electrode (GCE). GCE/CNNS–AuNPs (step A), GCE/CNNS–AuNPs/p-DNA (step B), GCE/CNNS–AuNPs/p-DNA/Dam/Dpn I (step C), and GCE/CNNS–AuNPs/p-DNA/Dam/Dpn I/CNNS (step D).

heavy-metal-containing quantum dots (QDs).[24−30] Several pioneering works in templating CN with nanopores[31] and chemically tailoring[32] and exfoliating[33] bulk CN into QDs/nanosheets have been reported, which further expands the scope of potential sensing applications of CN and improves the sensing performance. Moreover, compared to the very recent counterparts such as carbon/graphene/polymer dots that often exhibit defect luminescence, the nanostructured CN mostly shows band-gap luminescence; that is, the emission wavelength does not depend on the wavelength of excitation light.[32] As such, the unambiguous luminescence mechanism of CN would largely avoid the uncertainness in practical sensing applications as carbon/graphene/polymer dots meet, especially in complicated environments.

On the other hand, two general strategies have been reported to utilize the CN luminophor as the probe in ECL biosensors. One is to immobilize CN directly on the substrate electrode and subsequently assemble with functional molecules as recognition units that often inhibit the ECL of CN. When biological recognition event occurs, the amount of molecules that sit on the probe would inhibit the ECL of CN, and the signal decrease varies with the concentration of target molecules.[34,35] Such a signal-off strategy normally has a robust immobilization of CN probes. However, the maximum signal decrease is limited to 100% (complete quench) of original CN ECL intensity, which is not favorable for improving the sensitivity of the sensor. In the other strategy, the CN probe is captured during the recognition event that is often assembled at the last step of the modified electrode. A higher concentration of target molecules brings more amount of captured CN on the modified electrode, which will produce a stronger intensity of the ECL signal.[36,37] Of note, with respect to the signal-off strategy, there is more room to increase the ECL intensity for this method, which is advantageous to boost the sensing sensitivity. However, the monitoring of assembly processes often requires external electrochemical probes that may be irreversibly adsorbed and/or penetrated into the sensing interface, causing uncertain disruption of the biosensor. As each of them has their own characteristic set of advantages and limitations, both of these two popular ways have been individually applied to CN-based ECL biosensors as well as other photo-electrochemical biosensors.[38−40] However, to the best of our knowledge, the coupling of these two strategies in a single ECL biosensor that combines the advantages of each system has been rarely reported.

Herein, a sandwich-assembled electrode using multifunctional CN nanosheets (CNNS) is proposed to evaluate the Dam MTase activity (Figure 1). Except for being used as an excellent substrate for conjugating a large amount of hairpin probe DNA (p-DNA), the CNNS were successfully utilized as dual ECL signal reporters in both the bottom and top layers of the modified electrode, which were responsible for the biosensor reliability and concentration of analyte, respectively. Such a unique sandwich configuration not only offers a sensing performance superior to those of most previous MTase biosensors even using PCR/isothermal amplification techniques (Table 1), with a wide linear range of 0.05−80 U/mL and a detection limit down to 0.043 U/mL, but also enables an internal reliability self-check function during biosensing as usual without any supplementary chemicals.

EXPERIMENTAL SECTION

Chemicals and Materials. Dicyandiamide (DCDA, 99%), $HAuCl_4 \cdot 3H_2O$, and $K_2S_2O_8$ were purchased from Sigma-Aldrich. Dam methyltransferase (Dam MTase) supplied with 10× Dam methylase buffer, *S*-adenosyl methionine (SAM), Dpn I endonuclease supplied with 10× CutSmart buffer, M.SssI methyltransferase (M.SssI MTase) supplied with 10× NEBuffer 2, and hairpin DNA (5′-CAGAGATCCATATACGTTTTTCGTATATGGATCTCTGAAAAA-$(CH_2)_3$-SH-3′) were obtained from New England Biolabs (Ipswich, MA). Phosphate-buffered solution (PBS, 0.01 M, pH 7.4) used in this work was prepared using 137 mM NaCl, 10 mM Na_2HPO_4, and 2 mM KH_2PO_4. All other chemicals were of analytical grade and obtained from Sinopharm Chemical Reagent Co., Ltd. (Shanghai, China) unless otherwise specified. Ultrapure water (18.2 MΩ·cm at 25 °C, Thermo Scientific, USA) was used throughout the experiments.

Characterization. Transmission electron microscopy (TEM) images were recorded on a JEOL JEM-2100F transmission electron microscope (Japan) operated at 200 kV. UV−vis absorption spectra were measured with Cary 100 (Agilent, Singapore). PL measurements were performed on a FluoroMax-4 fluorescence spectrometer (HORIBA Jobin Yvon, Japan). ECL detection experiments were carried out on an MPI-E ECL analyzer system (Remex Electronic Instrument Lt. Co., Xi'an, China) with a three-electrode system containing a Pt wire as the

DOI: 10.1021/acsami.7b17813
ACS Appl. Mater. Interfaces 2018, 10, 6887−6894

Table 1. Comparison of Different Methods for Assay of the Dam Activity

detection techniques	methods	linear range (U/mL)	LOD (U/mL)	refs
fluorescence	fluorescent probes coupled with enzyme-linkage reactions	0.8−40	0.8	48
fluorescence	superquenching of aggregation-induced emission	0−20		49
fluorescence	label-free fluorometric biosensing based on perylene probe monomer-excimer transition	0.2−80		50
fluorescence[a]	hairpin-shaped DNAzyme	0.4−500	0.4	51
fluorescence[a]	exonuclease III-aided signal amplification	0.01−10	0.01	10
fluorescence[a]	versatile DNAzyme-based amplified biosensing	0.5−40	0.2	52
fluorescence[a]	label-free molecular beacon-mediated quadratic isothermal exponential amplification	0.0005−0.01	1.5×10^{-4}	53
UV−vis	enzyme-responsive nanoparticle system with a DNA−AuNP substrate	0−40		7
UV−vis	cation exchange of CuS nanoparticles and click chemistry of functionalized AuNPs	5−120		54
UV−vis[a]	methylation-responsive DNAzyme	0.25−400	0.25	55
electrochemistry	combining DNA methylation-sensitive cleavage and terminal transferase-mediated extension	0.1−20	0.04	56
electrochemistry	methylation-responsive hairpin-capture DNA probe	0.1−1	0.07	57
electrochemistry	controllable assembly of single-wall carbon nanotubes	0.1−1	0.04	58
DPV	discrimination of the aggregation of long and short DNA on a negatively charged indium tin oxide microelectrode	0.5−50	0.18	59
colorimetry	AuNPs coupled with enzyme-linkage reactions	1−10	0.3	8
chemiluminescence[a]	hybridization chain reaction-based branched rolling circle amplification	1−10	0.52	60
chemiluminescence[a]	hairpin probe-based primer generation rolling circle amplification	0.025−2.5	0.000129	11
TIRF images	a single QD-based nanosensor	0.004−2	0.002	61
SERS	mesoporous silica nanoparticle probe	0.1−10	0.02	62
SERS[a]	target-triggering primer generation-based multiple signal amplification	0.001−10	2.57×10^{-4}	63
ECL	GO/AgNP/luminol composites	0.1−20	0.03	9
ECL	quenching ECL of tris(2,2′-bipyridine) ruthenium using ferrocene	0.1−100	0.03	34
ECL	CNNS probe	0.05−80	0.043	this work

[a]PCR/isothermal amplification techniques were used.

counter electrode, Ag/AgCl (saturated KCl) as the reference electrode, and a bare or modified GCE as the working electrode. The supporting electrolyte was 0.01 M PBS (pH 7.4) with 0.1 M $K_2S_2O_8$ as the cathodic ECL coreactant. ECL emission was obtained by cyclic voltammetry within a potential window ranging from −1.3 to 0 V. The scan rate was 100 mV/s. Electrochemical impedance spectroscopy (EIS) was measured on Gamry Reference 600 potentiostat/galvanostat/ZRA (U.S.A).

Preparation of Bulk CN and CNNS. Bulk CN was synthesized according to previous procedures.[28] Briefly, 10 g of DCDA was put into a capped crucible and heated at 500 °C in air for 4 h at a 4 h ramp time. The nanosheets were obtained by liquid-phase exfoliating of the as-prepared bulk CN. Briefly, 100 mg of bulk CN was dispersed in 100 mL of water and then ultrasonicated for 16 h (KQ-400 KDE, 400 W, 40k HZ, China). The initial formed suspension was then centrifuged at 7000 rpm (Eppendorf Centrifuge 5415R) to remove the residual unexfoliated large particles before being used for further studies.

Preparation of CNNS−AuNPs and Control Samples (AuNPs and GO−AuNPs). CNNS−AuNPs[27] and GO−AuNPs[41] were prepared according to the previous procedures with a slight modification. For CNNS−AuNPs, briefly, 40 μL of $HAuCl_4$ (0.01 M) solution was added to 8 mL of the above prepared CNNS dispersion (ca. 0.1 mg/mL) under stirring. The obtained dispersion was then sonicated for 10 min, followed by stirring for 2 h at room temperature. The same process was repeated three times. Afterward, 40 μL of sodium citrate solution (0.01 M) was added dropwise into the dispersion, followed by stirring for 30 min. Then, 100 μL of freshly prepared $NaBH_4$ solution (0.01 M) was added quickly to the above dispersion, and the stirring reaction was maintained for 20 min. The obtained nanocomposite was centrifuged and washed three times with water to remove excess $NaBH_4$, sodium citrate, and unbound AuNPs. The final solid was redispersed in 1 mL of water and stored at 4 °C until use.

GO was prepared by a modified Hummers' method from natural graphite.[42] GO−AuNPs were synthesized according to previous procedures.[41,43−45] Briefly, after mixing 5 mL of 0.1 mg/mL GO dispersion (0.1 mg/mL) with 250 μL of $HAuCl_4$ (0.01 M) under stirring for 2 h, 250 μL of sodium citrate solution (0.01 M) was added dropwise into the dispersion, followed by stirring for 30 min. Then, 625 μL of freshly prepared $NaBH_4$ (0.01 M) was added quickly with the aid of ultrasonication for 30 min at room temperature. The obtained nanocomposite was centrifuged and washed three times with water to remove excess $NaBH_4$, sodium citrate, and unbound AuNPs. The final solid was redispersed in 1 mL of water and stored at 4 °C until use.

AuNPs were prepared by the citrate reduction of $HAuCl_4$.[46] Briefly, aqueous solution of $HAuCl_4$ (1 mM, 100 mL) was brought to reflux at continuous stirring, and then 10 mL of 38.8 mM sodium citrate solution was added quickly and kept boiling for another 15 min. This resulted in a change in the solution color from pale yellow to deep red. Then, the heating source was removed, and the dispersion was stirred for several minutes, allowed to cool to room temperature, and subsequently filtered through a Micron Separations Inc. 0.45 μm acetate filter. The as-obtained AuNPs solution was stored in brown bottles at 4 °C until use (Figure S1).

General Procedure for the Assembly of ECL Biosensors. Prior to modification, the GCE (d = 3 mm) was successively polished with 0.3 and 0.05 μm alumina slurry, then washed ultrasonically in anhydrous ethanol and ultrapure water, respectively, and dried in a N_2 atmosphere. Subsequently, 3 μL of the CNNS−AuNPs dispersion was drop-cast on the GCE. After the modified electrode was dried at room temperature, the free CNNS−AuNPs nanohybrid was rinsed out with PBS (0.01 M, pH 7.4). Then, 10 μL of hairpin DNA (4×10^{-7} M) solution was dropped onto the electrode and incubated for 2 h at 37 °C, followed by blocking with 2 mM 2-mercaptoethanol (MCH) for 40 min. The electrode was further incubated with 10 μL of appropriate buffer containing Dam MTase (0.5 μL) at 37 °C for 2 h to initiate the methylation reaction. Afterward, 10 μL of a solution containing appropriate buffer and Dpn I (10 U) was deposited dropwise on the electrode and incubated for 2 h at 37 °C. Finally, 5 μL of CNNS dispersion (ca. 0.1 mg/mL) was dropped on the electrode and incubated for 1 h at 37 °C. The uncaptured CNNS was rinsed out using PBS.

Selectivity and Inhibition Investigation of the Dam MTase Assay. M.SssI MTase was selected as the potential interfering enzyme. The selectivity experiments were conducted with 80 U/mL MTase in the same way as the Dam MTase activity detection procedure. To further study the inhibitor-screening ability of the proposed assay, the

DOI: 10.1021/acsami.7b17813
ACS Appl. Mater. Interfaces 2018, 10, 6887−6894

inhibition effect of 5-fluorouracil on the Dam MTase activity was investigated by incubating the hairpin DNA-coated electrode in 10× Dam buffer consisting of 80 U/mL Dam MTase and 160 μM SAM with various concentrations of the inhibitors.

RESULTS AND DISCUSSION

Immobilization of AuNPs on CNNS for Reliable Coupling Biomolecules. Figure 1 shows the general processes of assembling sandwiched CNNS ECL sensor for evaluation of the Dam MTase activity. Because of the chemical innerness of CNNS, to ensure a reliable connection between biomolecules and CNNS, AuNPs were first deposited on CNNS. For this, $HAuCl_4$ was first chemically adsorbed on CNNS by protonation and then reduced in situ using $NaBH_4$. The successful deposition of AuNPs on CNNS was first verified by the UV−vis absorption spectra. Compared to bare CNNS, an evident new absorption peak at ca. 520 nm (Figure 2a), corresponding to

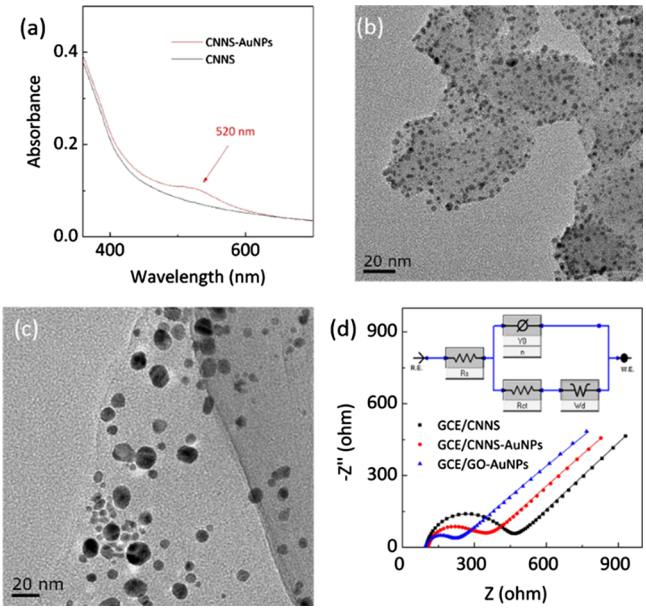

Figure 2. (a) UV−vis absorption spectra of CNNS and CNNS−AuNPs. (b) TEM image of CNNS−AuNPs. (c) TEM image of GO−AuNPs. (d) Nyquist plots (scatters) and simulation (lines) of CNNS, CNNS−AuNPs, and GO−AuNPs. The inset in (d) shows the equivalent Randles circuit.

the characteristic plasmon resonance of AuNPs, was observed for CNNS−AuNPs. The TEM images in Figures 2b and S2a further demonstrated that the AuNPs with an average size of ca. 3 nm (Figure S3) were homogeneously anchored on CNNS. No agglomeration of the AuNPs was observed, revealing that the formed AuNPs were tightly anchored to the inherent functional groups on the surface of CNNS. In contrast, similar to previous reports,[35,41,44,45] the AuNPs (see the absorption of plasmon resonance in Figure S4) of larger size and lower immobilization density were less homogeneously distributed on GO nanosheets (Figures 2c and S2b). Such an evident difference in the immobilization of AuNPs may be ascribed to the fact that the uniform distribution of N atoms with unpaired electrons in the framework of CN could adsorbed the AuNP precursor, that is, $HAuCl_4$, more homogeneously than the random oxygen-containing active sites by the conventional Hummers' method in GO preparation. In this regard, AuNPs were more homogeneously deposited on CNNS than on the GO substrate, which is supposed to conjugate more biomolecules in a more robust manner.

Moreover, it was noted that the electronic conductivity of CNNS was largely improved after being deposited with AuNPs, which is vital in electrochemical applications. Figure 2d shows the EIS spectra of GCE/CNNS, GCE/CNNS−AuNPs, and GCE/GO−AuNPs. The Nyquist diagrams of all electrodes consisted of a line at a low frequency and a semicircle at a high frequency, the diameter of which often indicates the charge-transfer resistance (R_{ct}).[35] As CNNS is a poor electrical conductor, the EIS spectra of GCE/CNNS exhibited a semicircle with the largest diameter (R_{ct} = 347.8 Ω) among them at a high frequency. Nevertheless, the semicircle was largely reduced after the deposition of AuNPs on the CNNS (R_{ct} = 233.0 Ω), approaching close to that of GO−AuNPs (R_{ct} = 128.5 Ω) on the same order of magnitude. Thus, as an extra benefit, the EIS results confirmed that much improved conductivity of the CNNS after the deposition of AuNPs was also achieved.

Assembling a Sandwich-CNNS-Based MTase ECL Biosensor with the Capability of Quality Self-Check. In general, the assembling of sandwich-structured MTase ECL biosensors includes four steps (Figure 1): (A) drop-cast of CNNS−AuNPs on a GCE both as the substrate for further coupling biomolecules and the quality self-check reporter, (B) conjugation of p-DNA via Au−S bonding as a connector, (C) methylation of the hairpin probe by the Dam MTase at the recognition site (5′-GATC-3′), yielding the methylated DNA probe, which was recognized and cleaved by Dpn I, and (D) capturing CNNS by the single-stranded DNA (ssDNA) left on the electrode as the MTase activity reporter because ssDNA has a much stronger noncovalent interaction with CNNS compared to the double-stranded DNA.[47] EIS was widely used to monitor each step of assembling because the surface properties and the charge-transfer resistance of the modified electrodes vary during the biosensor fabrication process. As shown in Figure 3a, the EIS

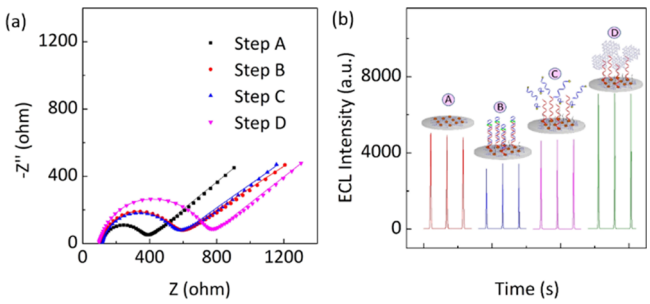

Figure 3. (a) Nyquist plots (scatters) and simulation (lines) and (b) ECL responses of GCE/CNNS−AuNPs (step A), GCE/CNNS−AuNPs/p-DNA (step B), GCE/CNNS−AuNPs/p-DNA/Dam/Dpn I (step C), and GCE/CNNS−AuNPs/p-DNA/Dam/Dpn I/CNNS (step D). Photomultiplier tube (PMT) voltage: 350 V.

spectra of GCE/CNNS−AuNPs (step A) exhibited a semicircle with a small diameter (R_{ct} = 277.0 Ω) at a high frequency. After p-DNA activation, p-DNA was bonded on the CNNS−AuNPs film via Au−S bonding, leading to an increase of R_{ct} (470.0 Ω) due to the poor conductivity of p-DNA (step B). The EIS spectra of GCE/CNNS−AuNPs/p-DNA/Dam/Dpn I slightly decreased (step C, R_{ct} = 460.0 Ω), suggesting that the steric hindrance decreased compared with that in the previous step, which could be attributed to the formation of ssDNA. R_{ct} (650.7 Ω) increased after the capture of CNNS (step D), which could be attributed to the greater steric hindrance.

Nevertheless, of note, similar to the cyclic voltammetry method, such EIS measurements need specific redox species as the probes,

DOI: 10.1021/acsami.7b17813
ACS Appl. Mater. Interfaces 2018, 10, 6887−6894

such as $Fe(CN)_6^{2+}/Fe(CN)_6^{3+}$. The external chemicals would not only make the sensing procedure complicated but also have risks in denaturing the assembled biomolecules because the universal electrostatic interactions and electric flow during the electrochemical measurements would make the redox probe unavoidable to adsorb on the surface or penetrate into the inner space of the assembled biomolecules. These potential side effects are largely overlooked in previous studies, and quality check is not applicable to each biosensor in fabrication, leading to erroneous results by the unqualified one. Therefore, it is highly anticipated to develop biosensors with the quality self-check ability without any external chemicals or tool kits, similar to a power-on self-test, a process performed by embedded firmware routines immediately after a computer or other digital electronic equipment is powered on to check if devices are functioning properly.

For this challenge, the ECL signals of the sandwich-structured ECL sensor during each assembly step (Figure 1) were recorded. As shown in Figure 3b, when CNNS−AuNPs were deposited on the GCE (step A), an evident ECL from CNNS was observed. After p-DNA was immobilized on CNNS−AuNPs through the Au−S bond and followed by the MCH blocking, the ECL intensity decreased (step B) because of the steric hindrance effect. With further interaction with Dam/Dpn I (step C), the ECL value was partially recovered, indicating that the hindrance decreased. After capturing top-layer CNNS via noncovalent interaction by ssDNA (step D), the ECL intensity increased significantly. It was noted that the ECL responses of each stage were in accordance with those of EIS results in Figure 3a. Moreover, except for coreactants and supporting electrolytes that were needed for sensing processes, no extra chemicals were introduced in the proposed biosensor system, and the ECL signal that was closely related to the quality of the biosensor was directly generated by the embedded bottom CNNS probe in the sandwiched biosensor. This suggested that we can facilely detect the reliability of biosensors similar to sensing target molecules, without introducing any extra chemicals. The advantage of this strategy was that it can largely avoid a series of unreliable problems during sensing procedures, such as uncertain failures in bioconjugation and the subsequent wrong readouts. Although a similar way was used to verify the successful fabrication of ECL and photoelectrochemical biosensors,[38−40] the concept of quality self-check for each biosensor to minimize the unqualified one in practical sensing has been rarely realized. It is supposed that the quality self-check function by the embedded probe without any extra additives in sensing could open up a new era for smart biosensors in practical applications.

Evaluation of the MTase Activity by the CNNS Sandwich-Structured ECL Sensor. The stability and intensity of the ECL signal would significantly influence the reliability and sensitivity of ECL biosensors. It was observed that the ECL intensities of GCE−CNNS−AuNPs were almost not changed under 20 continuous cyclic voltammetric scans between −1.3 and 0 V (Figure S5), indicating their high stability. Moreover, except for GCE/CNNS−AuNPs, the control substrate electrode including GCE/GO−AuNPs, GCE/AuNPs (i.e., merely using CNNS at the top layer; see D′ in Figure 1), and Au electrode was used to assemble the MTase biosensor. Under the same conductions, interestingly, GCE/CNNS−AuNPs exhibited the overwhelmingly strongest ECL intensity than other counterparts (Figure 4a). The uniform distribution of a high density of AuNPs with small particle sizes on CNNS not only enhanced the electronic conductivity of the CNNS emitter in the bottom layer but also improved the loading of probe DNA and

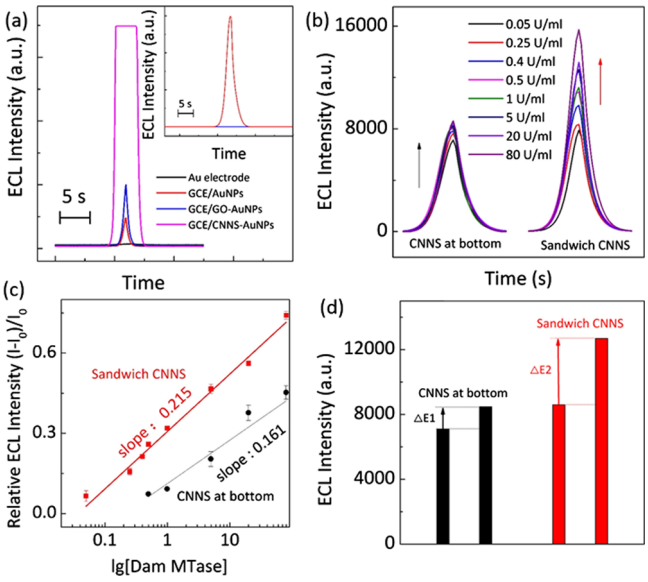

Figure 4. (a) ECL intensity of the MTase biosensors using different substrates (PMT voltage: 600 V). To get unoverflowed ECL, the PMT voltage was decreased to 350 V, which is shown in the inset. (b) ECL intensity obtained from the biosensors using the configuration of CNNS at the bottom (left) and the sandwich CNNS (right) triggered by different concentrations of Dam MTase. (c) Calibration curves of the biosensors using the configuration of CNNS at the bottom (black) and the sandwich CNNS (red), indicating that the latter offered superior linear range and detection limit. (d) ECL intensity change of the biosensors using the configuration of CNNS at the bottom (black) and the sandwich CNNS (red) at the same concentration of Dam MTase (5 U/mL), suggesting that the latter had higher sensitivity. PMT voltage: 350 V.

subsequent capturing of more CNNS probe by ssDNA at the top layer, an important factor for the enhanced performance of the MTase biosensor.

The relationship between the ECL intensity and the Dam MTase concentration was investigated. It was found that the ECL intensity increased with the increase of the Dam MTase concentration in the range of 0.05−80 U/mL (Figure 4b). A good linear relationship between the ECL intensity changes of step D and step C (Figure 1) and the Dam MTase concentration could also be obtained. The detection limit (LOD, S/N = 3) was estimated to be 0.043 U/mL (Figure 4c). Such sensing performances were superior to those in most previous reports even with PCR/isothermal amplification techniques, as shown in Table 1.

The high sensitivity of this sensor can be explained by the unique sandwiched structure of the CNNS. On the one hand, as discussed in Figure 4a, the CNNS−AuNPs worked as a better substrate (D in Figure 1) than bare GCE (D′ in Figure 1) and even GCE/GO−AuNPs to effectively immobilize hairpin probe,[64,65] which was favorable for improving the sensitivity. On the other hand, with respect to the signal-off strategy, there is more room for the captured amount of the CNNS probe by ssDNA in the top layer at the last step in sensor fabrication procedures (step D in Figure 1). Thus, it is highly anticipated that a much more boosted ECL intensity would be observed, with respect to the ECL recovery strategy that utilized the CNNS at the bottom layer (step C in Figure 1). To confirm this speculation, the ECL intensity change before (step B in Figure 1) and after (step C in Figure 1) the formation of ssDNA was also investigated. It was found that the ECL intensity also

DOI: 10.1021/acsami.7b17813
ACS Appl. Mater. Interfaces 2018, 10, 6887−6894

increased with the improvement of the Dam MTase concentration but with a lower slope and a much narrower linear range (0.5−80 U/mL). Moreover, it was noted that Dam MTase with the same concentration can cause much higher ECL intensity change of the sandwich-structured biosensor (Figure 4d). All of these performances of the CNNS sandwich-structured biosensor (D in Figure 1) are superior to those of traditional one that using the CNNS probe only at the bottom (C in Figure 1) or the top layer (D′ in Figure 1).

The specificity of the Dam MTase for the sandwich CNNS-based ECL biosensor was evaluated in the presence of only Dam MTase or Dpn I or using other type of MTase (M.SssI MTase + Dpn I) as an interfering control. It was found that at identical conditions, only in the presence of both Dam MTase and Dpn I, a significant ECL intensity change could be observed (Figure 5a), whereas those with M.SssI MTase + Dpn I and

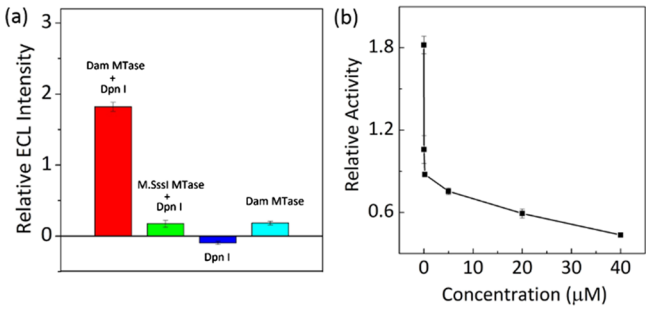

Figure 5. (a) Relative ECL intensity of the sandwich CNNS-based biosensor with Dam MTase + Dpn I, M.SssI MTase + Dpn I, merely Dpn I or Dam MTase under the same experimental conditions. (b) Inhibition effect of 5-fluorouracil on the Dam MTase activity. PMT voltage: 350 V.

merely Dam MTase or Dpn I were negligible. This was ascribed to the highly specific site recognition of Dam MTase and Dpn I toward their substrate, namely, the hairpin probe DNA in this study.[11] These results suggested that the proposed sandwich CNNS biosensor had excellent selectivity for Dam MTase by cooperating with Dpn I.

Except for playing an important role in the virulence of bacterial pathogens, Dam MTase, after the inhibition, also has potential applications in cancer therapy and antimicrobial drug development.[11] For this, the study of whether our simple and sensitive assay method can be employed for the screening of Dam MTase inhibitors was further undertaken. Herein, 5-fluorouracil was introduced to estimate the inhibition of the Dam MTase activity (80 U/mL, Figure 5b). It was observed that because of the weakened methylation-blocked effect, the relative ECL intensity was monotonically decreased with increasing concentrations of the inhibitors. Thus, the proposed sandwich CNNS biosensor was applicable to the Dam MTase activity inhibition investigation.

Detection of Dam MTase in Realistic Samples. The proposed ECL biosensor was also used to detect Dam MTase in human serum samples. Several ECL sensors were fabricated by incubation in the diluted normal human serum samples (diluted in a 1:10 ratio with 0.01 M pH 7.4 PBS). The recovery test was performed using the standard addition method.[14] As displayed in Table 2, for Dam MTase at different concentrations of 0.05, 0.5, 5, and 80 U/mL, there was a good agreement between the added and measured values of the Dam MTase concentrations, and the recoveries ranged from 97.4 to 113%, thereby validating the reliability and practicality of this method.

Table 2. Recovery Results of Dam MTase Added in 10% Human Serum Samples

entry	added (U/mL)	found (U/mL)	relative standard deviation (RSD) (%, N = 3)	recovery (%)
1	0.05	0.0566	2.28	113.0
2	0.5	0.5333	2.65	106.6
3	5	4.868	4.47	97.4
4	80	80.887[a]	5.34	101.1

[a]The sensing performances at the updetection range of the proposed sensor was tested. For this, 80 U/mL Dam MTase in human serum was undertaken. According to the calibration curve, 80.887 U/mL was obtained with acceptable RSD and recovery. Although it was very close to the actual values (only over 1.1%), it exceeded the detection range and should not be used in the practical detection.

CONCLUSIONS

In this work, a sandwich CNNS-based ECL biosensor was developed for the evaluation of the Dam MTase activity. It was revealed that the multifunctional CNNS could not only be used as a substrate to effectively immobilize biomolecules by being deposited with AuNPs so as to boost the sensitivity but also be utilized as an internal biosensor reliability checker and an analyte reporter in the bottom and top layers of the biosensor, respectively. Such a unique configuration coupled the advantages of the CNNS emitter in the conventional bottom or top layer. Our result also demonstrated the performance of the CNNS sandwich-structured ECL biosensor, which is superior to those of most biosensors in previous reports in sensing Dam MTase activity with an ultralow detection limit down to 0.043 U/mL and a linear range from 0.05 to 80 U/mL. This work would open a promising avenue to develop highly sensitive and smart quality self-testable ECL sensing systems using a sandwiched configuration of emerging CNNS luminophors for early disease diagnosis, treatment, and management.

ASSOCIATED CONTENT

Supporting Information

The Supporting Information is available free of charge on the ACS Publications website at DOI: 10.1021/acsami.7b17813.

TEM images of AuNPs, CNNS−AuNPs, and GO−AuNPs; particle size distribution of AuNPs; UV−vis absorption spectra of GO−AuNPs; ECL emission of CNNS−AuNPs; and supplementary discussion of high ECL background in Figure 3 (PDF)

AUTHOR INFORMATION

Corresponding Author

*E-mail: Yuanjian.Zhang@seu.edu.cn.

ORCID

Yanfei Shen: 0000-0003-0369-5920

Songqin Liu: 0000-0002-4686-5291

Yuanjian Zhang: 0000-0003-2932-4159

Author Contributions

§Equivalent contribution (S.C. and Y.L.).

Notes

The authors declare no competing financial interest.

ACKNOWLEDGMENTS

This work was supported by the National Natural Science Foundation of China (21775018, 21675022), the Natural Science Foundation of Jiangsu Province (BK20160028,

BK20170084), the Open Funds of the State Key Laboratory of Electroanalytical Chemistry (SKLEAC201703), and the Fundamental Research Funds for the Central Universities.

REFERENCES

(1) Jeltsch, A. Beyond Watson and Crick: DNA Methylation and Molecular Enzymology of DNA Methyltransferases. *ChemBioChem* **2002**, *3*, 274−293.
(2) Heithoff, D. M.; Sinsheimer, R. L.; Low, D. A.; Mahan, M. J. An essential role for DNA adenine methylation in bacterial virulence. *Science* **1999**, *284*, 967−970.
(3) Robertson, K. D. DNA methylation and human disease. *Nat. Rev. Genet.* **2005**, *6*, 597−610.
(4) Li, L.; Tao, L.; Lubet, R. A.; Steele, V. E.; Pereira, M. A. Modulation by budesonide of a CpG endonuclease in mouse lung tumors. *Carcinogenesis* **2007**, *28*, 1499−1503.
(5) Rebeck, G. W.; Samson, L. Increased spontaneous mutation and alkylation sensitivity of Escherichia coli strains lacking the ogt O6-methylguanine DNA repair methyltransferase. *J. Bacteriol.* **1991**, *173*, 2068−2076.
(6) Bergerat, A.; Guschlbauer, W.; Fazakerley, G. V. Allosteric and catalytic binding of S-adenosylmethionine to Escherichia coli DNA adenine methyltransferase monitored by 3H NMR. *Proc. Natl. Acad. Sci. U.S.A.* **1991**, *88*, 6394−6397.
(7) Song, G.; Chen, C.; Ren, J.; Qu, X. A Simple, Universal Colorimetric Assay for Endonuclease/Methyltransferase Activity and Inhibition Based on an Enzyme-Responsive Nanoparticle System. *ACS Nano* **2009**, *3*, 1183−1189.
(8) Liu, T.; Zhao, J.; Zhang, D.; Li, G. Novel Method to Detect DNA Methylation Using Gold Nanoparticles Coupled with Enzyme-Linkage Reactions. *Anal. Chem.* **2010**, *82*, 229−233.
(9) Zhao, H.-F.; Liang, R.-P.; Wang, J.-W.; Qiu, J.-D. One-pot synthesis of GO/AgNPs/luminol composites with electrochemiluminescence activity for sensitive detection of DNA methyltransferase activity. *Biosens. Bioelectron.* **2015**, *63*, 458−464.
(10) Xing, X.-W.; Tang, F.; Wu, J.; Chu, J.-M.; Feng, Y.-Q.; Zhou, X.; Yuan, B.-F. Sensitive Detection of DNA Methyltransferase Activity Based on Exonuclease-Mediated Target Recycling. *Anal. Chem.* **2014**, *86*, 11269−11274.
(11) Zeng, Y.-p.; Hu, J.; Long, Y.; Zhang, C.-y. Sensitive Detection of DNA Methyltransferase Using Hairpin Probe-Based Primer Generation Rolling Circle Amplification-Induced Chemiluminescence. *Anal. Chem.* **2013**, *85*, 6143−6150.
(12) Wang, Q.; Pan, M.; Wei, J.; Liu, X.; Wang, F. Evaluation of DNA Methyltransferase Activity and Inhibition via Isothermal Enzyme-Free Concatenated Hybridization Chain Reaction. *ACS Sens.* **2017**, *2*, 932−939.
(13) Zhang, X.; Zhang, B.; Miao, W.; Zou, G. Molecular-Counting-Free and Electrochemiluminescent Single-Molecule Immunoassay with Dual-Stabilizers-Capped CdSe Nanocrystals as Labels. *Anal. Chem.* **2016**, *88*, 5482−5488.
(14) Gao, W.; Liu, Z.; Qi, L.; Lai, J.; Kitte, S. A.; Xu, G. Ultrasensitive Glutathione Detection Based on Lucigenin Cathodic Electrochemiluminescence in the Presence of MnO2 Nanosheets. *Anal. Chem.* **2016**, *88*, 7654−7659.
(15) Zhao, M.; Chen, A.-Y.; Huang, D.; Zhuo, Y.; Chai, Y.-Q.; Yuan, R. Cu Nanoclusters: Novel Electrochemiluminescence Emitters for Bioanalysis. *Anal. Chem.* **2016**, *88*, 11527−11532.
(16) Feng, Y.; Dai, C.; Lei, J.; Ju, H.; Cheng, Y. Silole-Containing Polymer Nanodot: An Aqueous Low-Potential Electrochemiluminescence Emitter for Biosensing. *Anal. Chem.* **2016**, *88*, 845−850.
(17) Li, G.; Yu, X.; Liu, D.; Liu, X.; Li, F.; Cui, H. Label-Free Electrochemiluminescence Aptasensor for 2,4,6-Trinitrotoluene Based on Bilayer Structure of Luminescence Functionalized Graphene Hybrids. *Anal. Chem.* **2015**, *87*, 10976−10981.
(18) Gao, H.; Wang, X.; Li, M.; Qi, H.; Gao, Q.; Zhang, C. Proximity hybridization-regulated electrogenerated chemiluminescence bioassay of α-fetoprotein via target-induced quenching mechanism. *Biosens. Bioelectron.* **2017**, *98*, 62−67.
(19) Duan, R.; Zhou, X.; Xing, D. Electrochemiluminescence Biobarcode Method Based on Cysteamine−Gold Nanoparticle Conjugates. *Anal. Chem.* **2010**, *82*, 3099−3103.
(20) Zhang, M.; Wang, X. Two dimensional conjugated polymers with enhanced optical absorption and charge separation for photocatalytic hydrogen evolution. *Energy Environ. Sci.* **2014**, *7*, 1902.
(21) Shalom, M.; Inal, S.; Fettkenhauer, C.; Neher, D.; Antonietti, M. Improving Carbon Nitride Photocatalysis by Supramolecular Preorganization of Monomers. *J. Am. Chem. Soc.* **2013**, *135*, 7118−7121.
(22) Zhang, Y.; Antonietti, M. Photocurrent Generation by Polymeric Carbon Nitride Solids: An Initial Step towards a Novel Photovoltaic System. *Chem.—Asian J.* **2010**, *5*, 1307−1311.
(23) Zhang, W.; Albero, J.; Xi, L.; Lange, K. M.; Garcia, H.; Wang, X.; Shalom, M. One-Pot Synthesis of Nickel-Modified Carbon Nitride Layers Toward Efficient Photoelectrochemical Cells. *ACS Appl. Mater. Interfaces* **2017**, *9*, 32667−32677.
(24) Cheng, C.; Huang, Y.; Tian, X.; Zheng, B.; Li, Y.; Yuan, H.; Xiao, D.; Xie, S.; Choi, M. M. F. Electrogenerated Chemiluminescence Behavior of Graphite-like Carbon Nitride and Its Application in Selective Sensing Cu2+. *Anal. Chem.* **2012**, *84*, 4754−4759.
(25) Cheng, C.; Huang, Y.; Wang, J.; Zheng, B.; Yuan, H.; Xiao, D. Anodic Electrogenerated Chemiluminescence Behavior of Graphite-Like Carbon Nitride and Its Sensing for Rutin. *Anal. Chem.* **2013**, *85*, 2601−2605.
(26) Chen, L.; Zeng, X.; Dandapat, A.; Chi, Y.; Kim, D. Installing Logic Gates in Permeability Controllable Polyelectrolyte-Carbon Nitride Films for Detecting Proteases and Nucleases. *Anal. Chem.* **2015**, *87*, 8851−8857.
(27) Chen, L.; Zeng, X.; Si, P.; Chen, Y.; Chi, Y.; Kim, D.-H.; Chen, G. Gold Nanoparticle-Graphite-Like C3N4 Nanosheet Nanohybrids Used for Electrochemiluminescent Immunosensor. *Anal. Chem.* **2014**, *86*, 4188−4195.
(28) Zhou, Z.; Shang, Q.; Shen, Y.; Zhang, L.; Zhang, Y.; Lv, Y.; Li, Y.; Liu, S.; Zhang, Y. Chemically Modulated Carbon Nitride Nanosheets for Highly Selective Electrochemiluminescent Detection of Multiple Metal-ions. *Anal. Chem.* **2016**, *88*, 6004−6010.
(29) Feng, Q.-M.; Shen, Y.-Z.; Li, M.-X.; Zhang, Z.-L.; Zhao, W.; Xu, J.-J.; Chen, H.-Y. Dual-Wavelength Electrochemiluminescence Ratiometry Based on Resonance Energy Transfer between Au Nanoparticles Functionalized g-C3N4 Nanosheet and Ru(bpy)32+ for microRNA Detection. *Anal. Chem.* **2016**, *88*, 937−944.
(30) Ji, J.; Wen, J.; Shen, Y.; Lv, Y.; Chen, Y.; Liu, S.; Ma, H.; Zhang, Y. Simultaneous Noncovalent Modification and Exfoliation of 2D Carbon Nitride for Enhanced Electrochemiluminescent Biosensing. *J. Am. Chem. Soc.* **2017**, *139*, 11698−11701.
(31) Wang, Y.; Wang, X.; Antonietti, M.; Zhang, Y. Facile One-Pot Synthesis of Nanoporous Carbon Nitride Solids by Using Soft Templates. *ChemSusChem* **2010**, *3*, 435−439.
(32) Zhou, Z.; Shen, Y.; Li, Y.; Liu, A.; Liu, S.; Zhang, Y. Chemical Cleavage of Layered Carbon Nitride with Enhanced Photoluminescent Performances and Photoconduction. *ACS Nano* **2015**, *9*, 12480−12487.
(33) Zhang, X.; Xie, X.; Wang, H.; Zhang, J.; Pan, B.; Xie, Y. Enhanced Photoresponsive Ultrathin Graphitic-Phase C3N4 Nanosheets for Bioimaging. *J. Am. Chem. Soc.* **2012**, *135*, 18−21.
(34) Luo, X.; Li, Y.; Zheng, J.; Qi, H.; Liang, Z.; Ning, X. The determination of DNA methyltransferase activity by quenching of tris(2,2′-bipyridine)ruthenium electrogenerated chemiluminescence with ferrocene. *Chem. Commun.* **2015**, *51*, 9487−9490.
(35) Dong, Y.-P.; Zhou, Y.; Wang, J.; Zhu, J.-J. Electrogenerated Chemiluminescence Resonance Energy Transfer between $Ru(bpy)_3^{2+}$ Electrogenerated Chemiluminescence and Gold Nanoparticles/Graphene Oxide Nanocomposites with Graphene Oxide as Coreactant and Its Sensing Application. *Anal. Chem.* **2016**, *88*, 5469−5475.
(36) Zhou, H.; Han, T.; Wei, Q.; Zhang, S. Efficient Enhancement of Electrochemiluminescence from Cadmium Sulfide Quantum Dots by

DOI: 10.1021/acsami.7b17813
ACS Appl. Mater. Interfaces 2018, 10, 6887−6894

Glucose Oxidase Mimicking Gold Nanoparticles for Highly Sensitive Assay of Methyltransferase Activity. *Anal. Chem.* **2016**, *88*, 2976−2983.
(37) Deng, H.; Yang, X.; Yeo, S. P. X.; Gao, Z. Highly Sensitive Electrochemical Methyltransferase Activity Assay. *Anal. Chem.* **2014**, *86*, 2117−2123.
(38) Fan, G.-C.; Zhu, H.; Shen, Q.; Han, L.; Zhao, M.; Zhang, J.-R.; Zhu, J.-J. Enhanced photoelectrochemical aptasensing platform based on exciton energy transfer between CdSeTe alloyed quantum dots and SiO2@Au nanocomposites. *Chem. Commun.* **2015**, *51*, 7023−7026.
(39) Dai, H.; Zhang, S.; Hong, Z.; Lin, Y. A Potentiometric Addressable Photoelectrochemical Biosensor for Sensitive Detection of Two Biomarkers. *Anal. Chem.* **2016**, *88*, 9532−9538.
(40) Zang, Y.; Lei, J.; Zhang, L.; Ju, H. In Situ Generation of Electron Acceptor for Photoelectrochemical Biosensing via Hemin-Mediated Catalytic Reaction. *Anal. Chem.* **2014**, *86*, 12362−12368.
(41) Li, X.-R.; Li, X.-L.; Xu, M.-C.; Xu, J.-J.; Chen, H.-Y. Gold nanodendrities on graphene oxide nanosheets for oxygen reduction reaction. *J. Mater. Chem. A* **2014**, *2*, 1697−1703.
(42) Zhang, Y.; Fugane, K.; Mori, T.; Niu, L.; Ye, J. Wet chemical synthesis of nitrogen-doped graphene towards oxygen reduction electrocatalysts without high-temperature pyrolysis. *J. Mater. Chem.* **2012**, *22*, 6575.
(43) Wu, M.-S.; He, L.-J.; Xu, J.-J.; Chen, H.-Y. RuSi@Ru(bpy)32+/Au@Ag2S Nanoparticles Electrochemiluminescence Resonance Energy Transfer System for Sensitive DNA Detection. *Anal. Chem.* **2014**, *86*, 4559−4565.
(44) Lee, Y. H.; Polavarapu, L.; Gao, N.; Yuan, P.; Xu, Q.-H. Enhanced Optical Properties of Graphene Oxide−Au Nanocrystal Composites. *Langmuir* **2012**, *28*, 321−326.
(45) Vinodgopal, K.; Neppolian, B.; Lightcap, I. V.; Grieser, F.; Ashokkumar, M.; Kamat, P. V. Sonolytic Design of Graphene−Au Nanocomposites. Simultaneous and Sequential Reduction of Graphene Oxide and Au(III). *J. Phys. Chem. Lett.* **2010**, *1*, 1987−1993.
(46) Liu, Y.; Zhang, L.; Wei, W.; Zhao, H.; Zhou, Z.; Zhang, Y.; Liu, S. Colorimetric detection of influenza A virus using antibody-functionalized gold nanoparticles. *Analyst* **2015**, *140*, 3989−3995.
(47) Wang, Q.; Wang, W.; Lei, J.; Xu, N.; Gao, F.; Ju, H. Fluorescence Quenching of Carbon Nitride Nanosheet through Its Interaction with DNA for Versatile Fluorescence Sensing. *Anal. Chem.* **2013**, *85*, 12182−12188.
(48) Li, J.; Yan, H.; Wang, K.; Tan, W.; Zhou, X. Hairpin Fluorescence DNA Probe for Real-Time Monitoring of DNA Methylation. *Anal. Chem.* **2007**, *79*, 1050−1056.
(49) Chen, J.; Wang, Y.; Li, W.; Zhou, H.; Li, Y.; Yu, C. Nucleic Acid-Induced Tetraphenylethene Probe Noncovalent Self-Assembly and the Superquenching of Aggregation-Induced Emission. *Anal. Chem.* **2014**, *86*, 9866−9872.
(50) Wang, Y.; Chen, J.; Chen, Y.; Li, W.; Yu, C. Polymer-Induced Perylene Probe Excimer Formation and Selective Sensing of DNA Methyltransferase Activity through the Monomer−Excimer Transition. *Anal. Chem.* **2014**, *86*, 4371−4378.
(51) Tian, T.; Xiao, H.; Long, Y.; Zhang, X.; Wang, S.; Zhou, X.; Liu, S.; Zhou, X. Sensitive analysis of DNA methyltransferase based on a hairpin-shaped DNAzyme. *Chem. Commun.* **2012**, *48*, 10031.
(52) Zhao, X.-H.; Gong, L.; Zhang, X.-B.; Yang, B.; Fu, T.; Hu, R.; Tan, W.; Yu, R. Versatile DNAzyme-Based Amplified Biosensing Platforms for Nucleic Acid, Protein, and Enzyme Activity Detection. *Anal. Chem.* **2013**, *85*, 3614−3620.
(53) Xue, Q.; Wang, L.; Jiang, W. Label-free molecular beacon-based quadratic isothermal exponential amplification: a simple and sensitive one-pot method to detect DNA methyltransferase activity. *Chem. Commun.* **2015**, *51*, 13538−13541.
(54) Zhang, X. R.; Zhang, Y.; Chen, F. T.; Li, Y.; Zhang, S. S. Visual detection of single-nucleotide polymorphisms and DNA methyltransferase based on cation-exchange of CuS nanoparticles and click chemistry of functionalized gold nanoparticles. *Chem. Commun.* **2016**, *52*, 13261−13264.
(55) Li, W.; Liu, Z.; Lin, H.; Nie, Z.; Chen, J.; Xu, X.; Yao, S. Label-Free Colorimetric Assay for Methyltransferase Activity Based on a Novel Methylation-Responsive DNAzyme Strategy. *Anal. Chem.* **2010**, *82*, 1935−1941.
(56) Wu, H.; Liu, S.; Jiang, J.; Shen, G.; Yu, R. A sensitive electrochemical biosensor for detection of DNA methyltransferase activity by combining DNA methylation-sensitive cleavage and terminal transferase-mediated extension. *Chem. Commun.* **2012**, *48*, 6280.
(57) Su, J.; He, X.; Wang, Y.; Wang, K.; Chen, Z.; Yan, G. A sensitive signal-on assay for MTase activity based on methylation-responsive hairpin-capture DNA probe. *Biosens. Bioelectron.* **2012**, *36*, 123−128.
(58) Wang, Y.; He, X.; Wang, K.; Su, J.; Chen, Z.; Yan, G.; Du, Y. A label-free electrochemical assay for methyltransferase activity detection based on the controllable assembly of single wall carbon nanotubes. *Biosens. Bioelectron.* **2013**, *41*, 238−243.
(59) Wei, X.; Ma, X.; Sun, J.-j.; Lin, Z.; Guo, L.; Qiu, B.; Chen, G. DNA Methylation Detection and Inhibitor Screening Based on the Discrimination of the Aggregation of Long and Short DNA on a Negatively Charged Indium Tin Oxide Microelectrode. *Anal. Chem.* **2014**, *86*, 3563−3567.
(60) Bi, S.; Zhao, T.; Luo, B.; Zhu, J.-J. Hybridization chain reaction-based branched rolling circle amplification for chemiluminescence detection of DNA methylation. *Chem. Commun.* **2013**, *49*, 6906.
(61) Ma, F.; Liu, W.-j.; Tang, B.; Zhang, C.-y. A single quantum dot-based nanosensor for the signal-on detection of DNA methyltransferase. *Chem. Commun.* **2017**, *53*, 6868−6871.
(62) Wang, X.; Cui, M.; Zhou, H.; Zhang, S. DNA-hybrid-gated functional mesoporous silica for sensitive DNA methyltransferase SERS detection. *Chem. Commun.* **2015**, *51*, 13983−13985.
(63) Li, Y.; Yu, C.; Han, H.; Zhao, C.; Zhang, X. Sensitive SERS detection of DNA methyltransferase by target triggering primer generation-based multiple signal amplification strategy. *Biosens. Bioelectron.* **2016**, *81*, 111−116.
(64) Zhang, P.; Zhuo, Y.; Chang, Y.; Yuan, R.; Chai, Y. Electrochemiluminescent Graphene Quantum Dots as a Sensing Platform: A Dual Amplification for MicroRNA Assay. *Anal. Chem.* **2015**, *87*, 10385−10391.
(65) Qian, R.; Ding, L.; Yan, L.; Lin, M.; Ju, H. A Robust Probe for Lighting Up Intracellular Telomerase via Primer Extension To Open a Nicked Molecular Beacon. *J. Am. Chem. Soc.* **2014**, *136*, 8205−8208.

DOI: 10.1021/acsami.7b17813
ACS Appl. Mater. Interfaces 2018, 10, 6887−6894